Received April 29, 2025, accepted June 30, 2025, publication date for online-first November 12, 2025.

Original Research Article

Evaluating Hybrid Deep Learning and Traditional Methods for PET Image Reconstruction

Asma Benyelles* and Amel Korti

Biomedical Engineering Laboratory, Faculty of Technology, University of Abou Bekr Belkaid, Tlemcen, Algeria.

* Corresponding Author Email: asma.benyelles@univ-tlemcen.dz

ABSTRACT

Background and Objective: Positron Emission Tomography (PET) images typically exhibit high noise levels and limited spatial resolution. This paper presents a comparative investigation of traditional PET image reconstruction methods, including Filtered Back Projection (FBP), Algebraic Reconstruction Technique (ART), and Ordered Subset Expectation Maximization (OSEM), alongside hybrid approaches that incorporate deep learning techniques.

Methods: The deep learning approach employed in this work is based on Generative Adversarial Networks (GANs), a powerful framework well suited for inverse problems and image generation tasks such as PET reconstruction. This approach is tested on a publicly available dataset consisting of PET images stored in DICOM format. Performance is evaluated using two standard metrics: the Peak Signal-to-Noise Ratio (PSNR) and the Mean Squared Error (MSE).

Results: The results demonstrate that our proposed methods outperform existing approaches in terms of performance while requiring less reconstruction time. Quantitatively, the Peak Signal-to-Noise Ratio (PSNR) of the reconstructed images is approximately 50 dB. Qualitatively, the observed high image quality supports these quantitative findings.

Conclusion: Our proposed hybrid method is highly effective for noisy PET images, enabling accurate reconstruction and preserving pertinent information and regions of interest, thereby facilitating medical diagnosis.

Keywords—*Positron emission tomography, Deep learning, Generative adversarial networks, Image reconstruction, Evaluation.*

INTRODUCTION

A key field in contemporary medical imaging, nuclear medicine visualizes and examines physiological and pathological processes at the molecular level using low dosages of radioactive tracers—radiopharmaceuticals. Injected, ingested, or inhaled radiopharmaceuticals enter the body and emit gamma rays, detected by imaging tools such as gamma

cameras and positron emission tomography (PET) scanners. The obtained raw data provides vital information for diagnosing and tracking certain diseases through the spatial distribution of the radiotracer within tissues. However, converting this data into high-quality images suitable for clinical interpretation requires sophisticated reconstruction methods that minimize artefacts, reduce noise, and maintain anatomical accuracy. PET images are degraded and have a low signal-to-noise ratio due to short scan durations and low-dose radiotracers.[1,2]

Analytical and iterative techniques have traditionally dominated image reconstruction in nuclear medicine. One of the earliest and most frequently used methods, Filtered Back Projection (FBP), is quite sensitive to noise and experiences resolution loss despite employing mathematical filtering on projection data. Iterative reconstruction methods, such as the Algebraic Reconstruction Technique (ART) and Ordered Subsets Expectation Maximization (OSEM), were introduced to address these limitations by refining the reconstruction through multiple iterations. Although these techniques improve image quality and noise suppression, they remain computationally expensive and require careful parameter tuning to balance resolution and noise reduction.[3]

By introducing data-driven approaches capable of understanding complex visual patterns, Artificial Intelligence (AI), especially deep learning, has transformed medical image reconstruction by reducing noise, recovering fine structural features, and accelerating the reconstruction process. Convolutional Neural Networks (CNNs) and Generative Adversarial Networks (GANs), as examples of deep learning models, have demonstrated exceptional ability in improving image quality. Unlike conventional methods that rely on explicit mathematical models, deep learning–based solutions use vast datasets to derive optimal representations of medical images, making them highly adaptable to variations in data acquisition protocols and scanner characteristics.[4]

Apart from purely deep learning–based reconstruction techniques, hybrid approaches that combine artificial intelligence with traditional methodologies have emerged as promising alternatives. These hybrid methods deliver superior image fidelity, enhanced noise suppression, and reduced computational demands by leveraging the strengths of conventional algorithms—such as the robustness of iterative reconstruction—alongside the learning capabilities of neural networks. By integrating deep learning models into existing reconstruction systems, hybrid approaches offer a balanced solution that improves image quality while maintaining the interpretability and reliability of traditional methods.[5,6]

Ida Häggström et al. developed a deep learning network to address major challenges in Positron Emission Tomography (PET) image reconstruction.[7] Their approach, DeepPET, directly and rapidly reconstructs high-quality, quantitative PET images from sinograms using a deep convolutional encoder-decoder network. They created a large dataset of over 291,000 reference images by randomly selecting parameters derived from a whole-body digital phantom and simulating actual PET scans, thereby producing noisy sinogram data to train, validate, and test DeepPET. The findings showed that DeepPET generates higher-quality images than traditional methods. Requiring significantly less time than conventional reconstruction techniques, the study concludes that the end-to-end encoder-decoder network architecture can effectively produce high-quality PET images.

This research compares hybrid reconstruction methods with conventional and deep learning–based algorithms for scintigraphy imaging. We evaluate the effectiveness of hybrid approaches that integrate deep learning with traditional methods, compared to single deep learning models and analytical or iterative techniques. Key parameters such as noise suppression, resolution retention, computational efficiency, and clinical interpretability will guide the assessment of model performance. The objective is to determine whether hybrid methodologies can bridge the gap between traditional techniques and AI-driven reconstruction, thereby yielding more precise and reliable medical imaging solutions. The concluding section of this study will present our findings, highlighting the advantages and disadvantages of each strategy while exploring prospective avenues for AI-assisted reconstruction in nuclear medicine.

MATERIALS AND METHODS

This section details the database, hardware, software, and methods employed in this study.

Database

The database used in this study consists of 80,000 PET images in DICOM format, with a resolution of 128 × 128 pixels, sourced from the Parkinson's Progression Markers Initiative website.[8] For training, validation, and testing purposes, the dataset was divided into proportions of 70%, 15%, and 15%, respectively.

The database was converted into sinograms. We applied our GAN model to 70% of the training sinograms to capture sinogram characteristics, and then used the remaining data to validate and test the model.

Hardware Reconstruction

Reconstructions were performed on a high-performance workstation equipped with an Intel Core i9-13900K processor clocked at 5.8 GHz, providing 24 cores for maximum computational parallelism. Graphical processing power was supplied by an NVIDIA GeForce RTX 4090 graphics card with 24 GB of GDDR6X memory, which was essential for accelerating intensive deep learning operations and complex reconstructions. The workstation also included 128 GB of DDR5 RAM at 6,000 MHz, ensuring smooth handling of large datasets. Storage was managed by a 2 TB PCIe Gen4 NVMe SSD, enabling extremely fast data loading and writing times. This advanced hardware configuration was critical for minimizing reconstruction times and supporting the use of sophisticated deep learning models.

Software Implementation

Our reconstruction framework was developed using Python 3.8, leveraging a comprehensive set of libraries for deep learning and image processing. The core of the deep learning model, a Generative Adversarial Network (GAN), was built with PyTorch 1.x, enabling efficient training and deployment on GPU hardware. Data handling and numerical operations were managed using NumPy, while performance evaluation utilized torchmetrics. Image loading, preprocessing, and traditional reconstruction methods, such as the Radon transform and ART (Algebraic Reconstruction Technique), were implemented using scikit-image (skimage) and OpenCV (cv2). Visualization of results was performed with Matplotlib, and the training process was monitored using tqdm for progress bar visualization. This robust software stack enabled seamless integration of advanced deep learning techniques with established classical reconstruction algorithms[9].

Generative Adversarial Networks (GANs)

Generative Adversarial Networks (GANs), introduced in the early 2010s, are a class of machine learning models comprising two opposing convolutional neural networks: the generator and the discriminator. The generator aims to synthesize sinograms from the input database, striving to produce outputs that closely resemble authentic sinograms. The discriminator evaluates input sinograms to determine their authenticity, distinguishing between real and generated data. The GANs equation is presented in Equation (1).

$$Min_G Max_D f(D,G) = E_x\left[\log\left(D(x)\right)\right] + E_z\left[\log\left(1 - D\left(G(z)\right)\right)\right] \quad (1)$$

In this context, E_x denotes the expected value across all real sinograms; $D_{(x)}$ represents the Discriminator's probability estimate that input x is real; $G_{(z)}$ represents the output of the Generator for noise z; $D(G_{(z)})$ represents the Discriminator's probability estimate for the authenticity of the generated sinograms; and E_z indicates the expected value across the Generator's entire random input space.

The architecture consists of two main components: a generator *(G)*, designed to create images intended to fool the discriminator, and a discriminator *(D)*, designed to distinguish between real and synthetically generated images. The generator G defines a probability distribution representing the distribution of its produced samples $G_{(z)}$ given a latent variable distribution z–pz. The primary goal of a GAN is to train the generator's distribution to closely approximate the actual data distribution. A shared loss function for both *D* and *G* enables a GAN to be optimized through simultaneous minimization and maximization.[10]

After applying our GAN model, we obtain enhanced sinograms, which are then reconstructed into images using traditional reconstruction methods such as Filtered Back Projection (FBP), Algebraic Reconstruction Technique

(ART), and Ordered Subset Expectation Maximization (OSEM), as presented in the following sections.

Filtered Back Projection (FBP)

Filtered Back Projection (FBP) is a fundamental and computationally straightforward analytical technique for tomographic image reconstruction. The method typically involves applying a ramp filter and windowing to attenuate noise, correcting for blurring by filtering the projection data (sinogram) in the frequency domain. The reconstructed image is then generated by back-projecting these filtered projections onto the image grid.[11]

$$f(x,y)=\int_0^{\pi}[P(\theta,r)*h(r)]_{r=x\cos(\theta)+y\sin(\theta)}d\theta \quad (2)$$

The FBP equation reconstructs the image value *f(x-,y)* at each point from the projection data *P(θ,r)*, also known as the sinogram. This process involves filtering each projection with a kernel *h(r)* (or |ω| in the frequency domain) and then summing these filtered contributions over all angles (integrating over *θ*).

Algebraic Reconstruction Technique (ART)

The Algebraic Reconstruction Technique (ART) is an early iterative method for image reconstruction. Starting with an initial image estimate, ART iteratively updates pixel values along projection rays to minimize the difference between the observed and projected data.[12]

$$p_i=\sum_{j=1}^{N}w_{ij}f_j \; for \; i=1,\ldots M \quad (3)$$

In the linear system used by ART for reconstruction, *pi* represents the i^{th} projection measurement, f_j denotes the value of the j^{th} pixel, and w_{ij} is a weight indicating the contribution of the j^{th} pixel to the i^{th} measurement, such as the extent of intersection between projection ray *i* and pixel *j*.

Ordered Subset Expectation Maximization (OSEM)

Primarily used in Positron Emission Tomography (PET) and Single-Photon Emission Computed Tomography (SPECT) emission tomography (PET, SPECT), Ordered Subsets Expectation Maximization (OSEM) is an accelerated iterative statistical reconstruction method. OSEM, a faster variant of the Expectation Maximization (EM) algorithm, processes ordered subsets of projection data in each iteration to improve convergence speed, updating the image estimate based on these subsets.[13]

$$f_j^{(k+1)}=\frac{f_j^{(k)}}{\sum_{i\in S_m}aij}\sum_{i\in S_m}aij\frac{g_i}{\sum_l ailf_l^{(k)}} \quad (4)$$

This equation shows how the current estimate $f_j^{(k)}$ is adjusted based on the ratio of measured projections g_i to estimated projections, weighted by the system matrix a_{ij} for the current subset S_m.

The quality of final images was evaluated using Mean Squared Error (MSE) and Peak Signal to Noise Ratio (PSNR).

Mean Squared Error (MSE)

The Mean Squared Error (MSE) is a commonly used and straightforward metric that quantifies the difference between the test image and the reconstructed image. It is defined by the following equation:[14]

$$MSE=\frac{1}{N\cdot M}\sum_{i=1}^{M}\sum_{j=1}^{N}\left(f(i,j)-f'(i,j)\right)^2 \quad (5)$$

where *f(i,j)* is the original image; *f'(i,j)* is the degraded image; *M* and *N* refer to the number of rows and columns, respectively.

Peak Signal to Noise Ratio (PSNR)

The performance of the proposed method is evaluated using the Peak Signal-to-Noise Ratio (PSNR) and the Mean Squared Error (MSE). The perceptual quality metric, PSNR, is calculated by comparing the reconstructed image with the original image.[15] The equations used to assess these performance measures are:

$$PSNR=\frac{10\log_{10}\left(I(i,j)\right)^2_{max}}{MSE} \quad (6)$$

where *I(i,j)* is the original image; $I(i,j)_{max}$ is the highest intensity value, *I* is the original image; and *MSE* is the mean squared error.

The next section details and shows a schematic illustration of our proposed method.

Proposed Method

A key obstacle in applying supervised learning to PET imaging is the difficulty of acquiring a large collection of high-quality scans in clinical practice, which is why the process begins with an input sinogram derived from an image.

The training dataset, representing 70% of the total database, was first converted into sinograms using the Radon transform. A GAN architecture, based on a deep convolutional structure, was applied to these sinograms for enhancement. This architecture consists of a Generator and a Discriminator. The Discriminator processes the sinograms to distinguish between real and generated data, outputting a probability score through a Sigmoid activation function in its final layer. The training of both networks involved optimizing their parameters using the Adam algorithm, a widely used adaptive method known for its efficiency and robustness. Training was conducted for 100 epochs, allowing the networks to learn and converge over the entire dataset multiple times.

The Generator consists of six two-dimensional convolutional layers with a fixed kernel size and padding to preserve the spatial dimensions of the input throughout the network. The input to the Generator is a tensor of dimension (N, 1, H, W). This input is processed by the first convolutional layer (conv1), followed by Instance Normalization and a Parametric Rectified Linear Unit (PReLU) activation function, which provides greater flexibility compared to the standard Rectified Linear Unit (ReLU). The subsequent layers follow a similar structure up to the residual connection, where the output of the last convolution is added to the original input of the Generator. This residual connection facilitates training and can enhance the quality of generated sinograms by preserving low-level information.

After completing the training phase, the performance of the trained GAN model was evaluated on a separate test dataset. The test images were first converted into sinograms and then enhanced using the GAN to achieve improved quality and reduced noise.

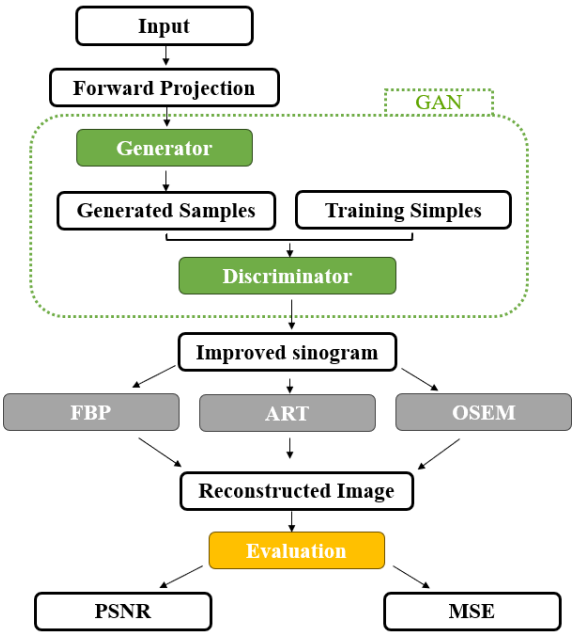

FIGURE 1. Schematic illustration of the hybrid deep learning method for PET data: They are separated into three sections; denoising of sinogram using GAN, reconstruction methods (FBP, ART, and OSEM), and evaluation with MSE and PSNR.

The enhanced sinogram is then input into traditional reconstruction algorithms: Filtered Back Projection (FBP), Algebraic Reconstruction Technique (ART), and Ordered Subsets Expectation Maximization (OSEM). The resulting reconstructed images are quantitatively evaluated using Peak Signal-to-Noise Ratio (PSNR) and Mean Squared Error (MSE) metrics to assess the effectiveness of GAN-based sinogram enhancement in improving reconstruction quality across different algorithms. Figure 1 illustrates the proposed method.

The next section details both the numerical and descriptive findings obtained using the methods mentioned previously.

RESULTS

This section presents the quantitative and qualitative results obtained from our proposed GAN model prior to reconstruction using the three traditional methods.

Three sinograms were selected to evaluate the proposed GAN model. Figures 2 and 3 show the reconstructed

images, and Table 1 presents the comparison results obtained using the evaluation metrics.

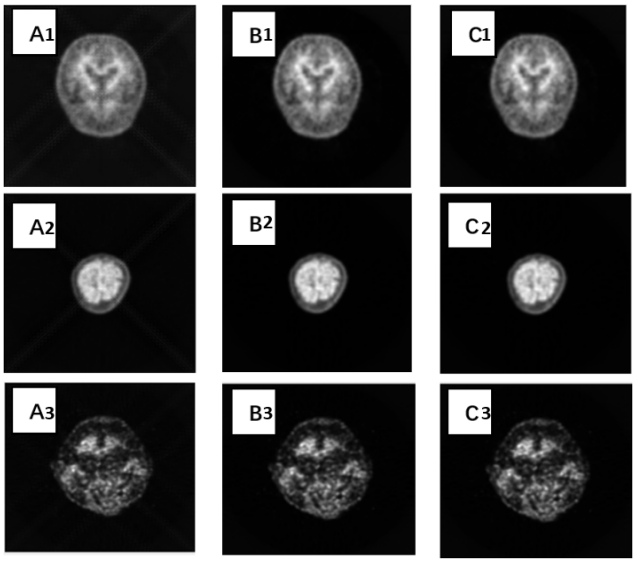

FIGURE 2. Schematic illustration of the hybrid deep learning method for PET data. The process is divided into three sections: denoising of the sinogram using GAN, reconstruction methods (FBP: column A, ART: column B, and OSEM: column C), and evaluation with MSE and PSNR.

TABLE 1. Values of PSNR, MSE, and reconstruction time for the proposed GAN model and the DeepPET model.

	EVALUATION		
	PSNR	**MSE**	**TIME(S)**
GAN-FBP	53.1906 54.2026 53.1381	$1.82e^{-5}$ $1.77e^{-5}$ $1.85e^{-5}$	3.45 3.48 3.44
GAN-ART	52.1756 51.5336 52.9978	$1.43e^{-5}$ $1.47e^{-5}$ $1.52e^{-5}$	5.56 5.76 5.88
GAN-OSEM	55.4581 55.7497 55.8165	$1.44e^{-5}$ $1.31e^{-5}$ $1.49e^{-5}$	9.69 9.89 9.08
DeepPET-FBP	51.7503 53.9884 54.5005	$1.53e^{-5}$ $1.49e^{-5}$ $1.52e^{-5}$	10.08 9.75 10.1
DeepPET-ART	52.2001 54.62 54.3875	$1.52e^{-5}$ $1.48e^{-5}$ $1.49e^{-5}$	11 11.5 11.31
DeepPET-OSEM	53.3665 54.004 55.1297	$1.51e^{-5}$ $1.5e^{-5}$ $1.47e^{-5}$	11.33 12.5 12.2

Figure 2 shows the datasets reconstructed using the three proposed hybrid methods. The GAN was applied to the sinogram of each image to enhance quality and reduce artifacts. These enhanced sinograms were then reconstructed using traditional methods and evaluated using PSNR and MSE metrics. Three distinct objects, differing in size, shape, and density, were selected to assess the range of results achievable with our proposed methodology. The statistical results are presented in Table 1.

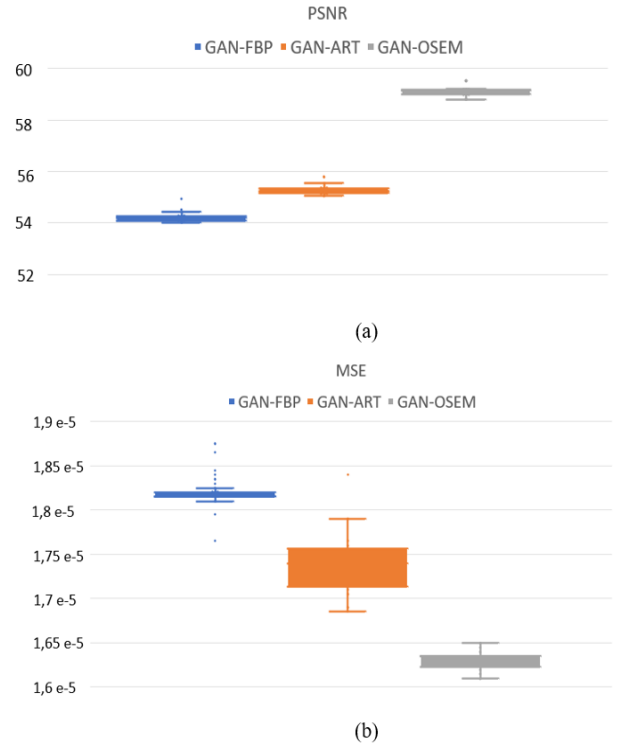

FIGURE 3. The variation of PSNR (a) and MSE (b) across 12,000 test images for GAN-FBP, GAN-ART, and GAN-OSEM.

Table 1 presents the PSNR and MSE values, along with the reconstruction time for each approach. The selection of these metrics is motivated by several factors. In PET imaging, accurate measurement of tracer uptake is crucial; MSE allows assessment of how well the reconstruction method preserves quantitative information within the images. Considering the inherently noisy nature of PET images, PSNR evaluates the effectiveness of the reconstruction technique in suppressing noise while maintaining the radiotracer distribution signal.

Figure 3 illustrates the variation of PSNR (a) and MSE (b) across 12,000 test images in our database for GAN-FBP, GAN-ART, and GAN-OSEM.

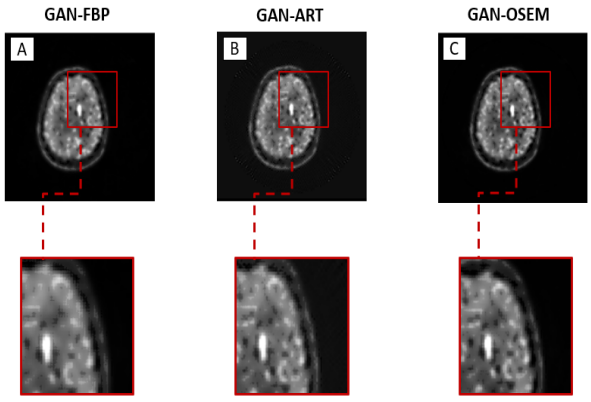

FIGURE 4. Examples of denoised PET images using emerging methods. Each column (A) to (C) shows the same PET slice. From left to right, the reconstructed results are from GAN-FBP, GAN-ART, and GAN-OSEM.

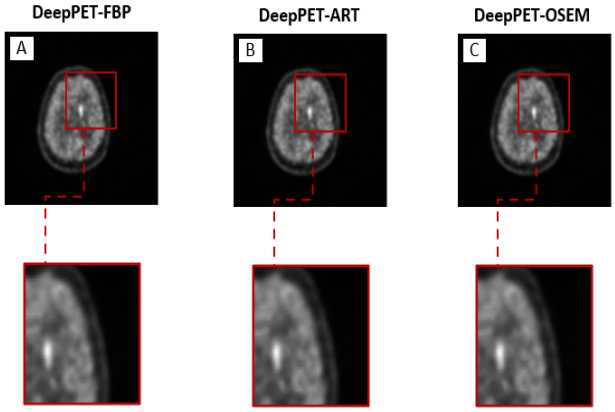

FIGURE 5. Examples of denoised PET images using the DeepPET method. Each column (A) to (C) shows the same PET slice. From left to right, the reconstructed results are from DeepPET-FBP, DeepPET-ART, and DeepPET-OSEM.

To validate our proposed GAN model, we compare it with the DeepPET model and obtain the results in Figure 4.

Figures 4 and 5 display the same brain scan reconstructions using different methods: FBP, ART, and OSEM. Each method presents both a full image and a zoomed-in view of a specific region, allowing for visual comparison of reconstruction quality. The results highlight the differences between DeepPET and the proposed method in terms of reconstructed image quality.

DISCUSSION

The performance of the proposed deep learning–enhanced reconstruction methods—GAN-OSEM, GAN-FBP, and GAN-ART—was comprehensively evaluated on a dataset of 12,000 images using PSNR and MSE as the primary metrics.

For the GAN-OSEM approach, PSNR values remained consistently high, ranging from approximately 54.2 dB to 55.8 dB, with most values clustered around 55.0 dB, indicating excellent overall image quality. Correspondingly, MSE values for GAN-OSEM were notably low, generally fluctuating between 1.25×10^{-5} and 1.55×10^{-5}. The relatively narrow spread for both metrics suggests robust and stable performance across the entire dataset, with minimal extreme variations.

For GAN-FBP, PSNR values were generally lower than those observed with GAN-OSEM, ranging from approximately 53.5 dB to 55.25 dB, with a mean around 54.0 dB. MSE values for GAN-FBP were higher, typically between 1.65×10^{-5} and 1.95×10^{-5}, indicating a greater average reconstruction error compared to GAN-OSEM. While performance remained strong, the slightly wider spread of data points suggests a marginally less consistent output quality.

For the GAN-ART method, PSNR values showed the lowest range among the three approaches, varying approximately between 52.0 dB and 55.0 dB, with most values concentrated around 53.0–53.5 dB. MSE values for GAN-ART were also the highest, typically ranging from 1.2×10^{-5} (with this lower bound appearing as an outlier, as most values exceeded 1.3×10^{-5}) to 2.0×10^{-5}, indicating the largest reconstruction errors. Despite having the lowest mean PSNR and highest mean MSE, the visual distribution for GAN-ART appeared relatively stable, although at a lower performance level compared to the other two methods.

Overall, the visual analysis of these 12,000 data points demonstrates that GAN-OSEM consistently achieves the highest PSNR and lowest MSE, indicating superior image reconstruction quality and precision. GAN-FBP follows, offering good performance but with slightly higher errors, while GAN-ART, although still effective, consistently produces the lowest PSNR and highest MSE among the

three hybrid approaches. The observed fluctuations across all 12,000 images for each method underscore the importance of evaluating performance over large datasets to capture the full range of metric variation.

The GAN-FBP method we propose is computationally efficient compared to iterative techniques. It offers a quick reconstruction process, is easy to implement, and tends to be robust and stable. Our technique provides satisfactory results even with noisy data, making it suitable for situations where noise is not a major concern. In situations where rapid image reconstruction is crucial, GAN-FBP is often the preferred choice.

The distinguishing characteristic of the GAN-ART algorithm lies in its adaptability, as it is capable of processing several forms of tomographic data. Our approach incrementally enhances the solution with each iteration, resulting in improved convergence. GAN-ART can generate scenarios to fill in missing projections or views in the data, allowing for more accurate reconstructions. Additionally, this method is flexible and can be applied to various imaging system geometries and configurations, resulting in faster reconstructions, particularly for large datasets.

The GAN-OSEM technique we employ utilizes code to implement the OSEM denoising algorithm for PET image reconstruction based on deep learning enhancement. This process is carried out iteratively over subsets, with the image being updated based on the ratio of measured and estimated sinograms.

The DeepPET model by Ida Häggström et al.,[7] applied to the sinogram and then reconstructed using traditional techniques, shows remarkable results in terms of noise and blur reduction but remains limited by the data in our database, which are voluminous, as it takes longer to reconstruct compared to our proposed methods. Figures 4 and 5 illustrate the differences between the four methods studied in this article and perceptually validate our results.

The evaluation of the reconstruction quality is performed using PSNR and MSE metrics. This method yields superior outcomes due to its iterative nature, which facilitates incremental enhancement of image quality and results in more precise reconstruction, especially in situations with low data counts. GAN-OSEM is proficient in addressing diverse systematic errors and artifacts encountered in PET imaging, including attenuation, scatter, and random events. The GAN-OSEM algorithm iteratively rectifies these effects, thereby enhancing image quality.

Traditional direct methods are unable to recover all pertinent information during the transformation of the sinogram into images, consequently leading to a loss of object details, contour definition, and regions of interest. This results in a significantly reduced signal-to-noise ratio. In contrast, these hybrid methods incorporating deep learning enable the generation of missing information, thereby ensuring good quality in the reconstructed images. The obtained results confirm that the hybrid approach is more effective than traditional methods, demonstrating a higher signal-to-noise ratio across all three proposed methods. Notably, GAN-OSEM clearly outperforms the other two. It is important to acknowledge that our proposed algorithm possesses limitations, such as the necessity for very large quantities of training data to effectively distinguish between generated and real sinograms. Despite its adaptability to various object types and shapes and its robustness, our method still requires further improvement to accommodate images from other modalities, aiming toward a more generalized algorithm. Another limitation of this study is that the validation only used an online database. In future studies, we plan to validate the results using a regional real-data database. We will also work on generalizing our algorithm to other modalities, such as MRI and CT, to better adapt the denoising and reconstruction method for large amounts of data.[16]

CONCLUSION

We conducted a comparative study for PET image denoising and reconstruction using deep learning with traditional methods, which demonstrates that the hybrid GAN-OSEM method yields qualitatively and quantitatively promising results, exhibiting reduced reconstruction time compared to traditional approaches and minimal noise and blurring in the reconstructed images. This methodology proves efficacious in the context of voluminous and noisy DICOM images, enabling effective reconstruction and the preservation of pertinent information and regions of interest, thereby facilitating medical diagnosis. The use

of deep learning is expected to be crucial in enhancing the performance of PET imaging as well as image processing.[17]

While our evaluation has demonstrated the robustness of the algorithm on a large set of clinical data, a more in-depth characterization of its intrinsic performance in terms of spatial resolution and contrast could be obtained through complementary studies. In this regard, the use of phantom images, such as the Jaszczak phantom, would be relevant for a controlled analysis of reconstruction capabilities. Furthermore, the evaluation of the Modulation Transfer Function (MTF) is envisioned to objectively quantify the resolution of the reconstructed image and will constitute a key direction for our future work.

AUTHOR CONTRIBUTIONS

Conceptualization, A.B. and A.K.; Methodology, A.B.; Software, A.B.; Hardware, A.B., Validation, A.K.; Formal Analysis, A.B.; Investigation, A.B.; Resources, A.B.; Data Curation, A.B.; Writing–Original Draft Preparation, A.B.; Writing–Review & Editing, A.B.; Visualization, A.B.; Supervision, A.K.; Project Administration, A.K.

ACKNOWLEDGMENTS

Not applicable.

FUNDING

This research received no external funding.

DATA AVAILABILITY STATEMENT

Not applicable.

CONFLICTS OF INTEREST

The authors declare they have no competing interests.

ETHICS APPROVAL AND CONSENT TO PARTICIPATE

Not applicable.

CONSENT FOR PUBLICATION

Not applicable.

FURTHER DISCLOSURE

Not applicable.

REFERENCES

1. Wang, Y., Li, E., Cherry, S.R., et al. Total-body PET kinetic modeling and potential opportunities using deep learning. *PET Clin*. 2021;16(4):613–625. https://doi.org/10.1016/j.cpet.2021.06.009.
2. Hashimoto, F., Ote, K., Onishi, Y. PET image reconstruction incorporating deep image prior and a forward projection model. *IEEE Trans Radiat*. 2022;6(8):841–846. https://doi.org/10.1109/TRPMS.2022.3161569.
3. Gong, K., Guan, J., Kim, K., et al. Iterative PET image reconstruction using convolutional neural network representation. *IEEE Trans Med Imaging*. 2019;38(3):675–685. https://doi.org/10.1109/TMI.2018.2869871.
4. Yi, X., Walia, E., Babyn, P.S. Generative adversarial network in medical imaging: a review. *Med Image Anal*. 2019;58(2):101552. https://doi.org/10.1016/j.media.2019.101552.
5. Andersen, A.H. and Kak, A.C. Simultaneous algebraic reconstruction technique (SART): a superior implementation of the ART algorithm. *Ultrason Imaging*. 1984;6(1):81–94. https://doi.org/10.1016/0161-7346(84)90008-7.
6. Long, Y., Huo, X., Liu, H., et al. An extended simultaneous algebraic reconstruction technique for imaging the ionosphere using GNSS data and its preliminary results. *Remote Sens*. 2023;15(11):2939. https://doi.org/10.3390/rs15112939.
7. Häggström, I., Schmidtlein, C.R., Campanella, G., et al. DeepPET: a deep encoder-decoder network for directly solving the PET image reconstruction inverse problem. *Med Image Anal*. 2019;54:253–262. https://doi.org/10.1016/j.media.2019.03.013.
8. Parkinson's Progression Markers Initiative (PPMI). Available online: https://www.ppmi-info.org/.
9. ARAMIS Project-Team. Algorithms, models and methods for images and signals of the human brain. Inria Paris Centre, CNRS, INSERM, Sorbonne Université, France, 2023. Available online: https://radar.inria.fr/rapportsactivite/RA2023/aramis/ARAMIS-RA-2023.pdf.
10. Wang, Z., She, Q., Ward, T.E. Generative adversarial networks in computer vision: a survey and taxonomy. Preprint. 2019, arXiv:1906.01529. Available online: https://arxiv.org/abs/1906.01529.
11. Beckmann, M. and Nickel, J. Optimized filter functions for filtered back projection reconstructions. https://doi.org/10.3934/ipi.2025003.

12. Hartling, K., Mahoney, F., Rand, E.T., et al. A comparison of algebraic reconstruction techniques for a single-detector muon computed tomography system. *Nucl Instrum Methods Phys Res A*. 2021;987:164834. https://doi.org/10.1016/j.nima.2020.164834.
13. Zeng, T., Gao, J., Gao, D. A GPU-accelerated fully 3D OSEM image reconstruction for a high-resolution small animal PET scanner using dual-ended readout detectors. *Phys Med Biol*. 2020;65(24). https://doi.org/10.1088/1361-6560/aba6f9.
14. Anaya-Sánchez, H., Altamirano Robles L., Díaz Hernández, R., et al. WGAN-GP for synthetic retinal image generation: enhancing sensor-based medical imaging for classification models. *Sensors*. 2024;25(1):167. https://doi.org/10.3390/s25010167.
15. Al-Najjar, Y. Comparative analysis of image quality assessment metrics: MSE, PSNR, SSIM and FSIM. *Int J Sci Res*. 2024;13(3):110–114. https://doi.org/10.21275/SR24302013533.
16. Hashimoto, F., Onishi, Y., Ote, K., et al. Deep learning-based PET image denoising and reconstruction: a review. *Radiol Phys Technol*. 2024;17:24–46. https://doi.org/10.1007/s12194-024-00780-3.
17. He, W., Zhao, Y., Zhao, X., et al. A CNN-based four-layer DOI encoding detector using LYSO and BGO scintillators for small animal PET imaging. *Phys Med Biol*. 2023;68(9). https://doi.org/10.1088/1361-6560/accc07.